Chem Soc Rev

Harnessing Surface Structure to Enable High-Performance Cathode Materials for Lithium-ion Batteries

Journal:	*Chemical Society Reviews*
Manuscript ID	CS-TRV-02-2020-000137.R1
Article Type:	Tutorial Review
Date Submitted by the Author:	06-May-2020
Complete List of Authors:	Yang, Luyi; Peking University Shenzhen Graduate School, Yang, Kai; School of Advanced Materials, Peking University, Shenzhen Graduate School Zheng, Jiaxin; School of Advanced Materials, Peking University Shenzhen Graduate School Xu, Kang; US Army Research Laboratory Amine, Khalil; Argonne National Laboratory, Pan, Feng; Peking University, School of Advanced Materials

SCHOLARONE™
Manuscripts

Please do not adjust margins

ARTICLE

Harnessing Surface Structure to Enable High-Performance Cathode Materials for Lithium-ion Batteries

Received 00th January 20xx,
Accepted 00th January 20xx

DOI: 10.1039/x0xx00000x

Luyi Yang,[a] Kai Yang,[a] Jiaxin Zheng,[a] Kang Xu,[b] Khalil Amine[c] and Feng Pan*[a]

The ever-increasing demand for high-performance batteries have been driving the fundamental understanding of the crystal/surface structural and electrochemical properties of intercalation cathode materials, among which the olivine-type, spinel and layered lithium transition metal oxide materials have received particular attention in the past decade due to their successful commercializations. While the most current studies focus on the macroscopic and bulk crystal structure of these materials, our previous work suggests that, as a confined region where charge transfer takes place, the interfacial structures of cathode materials largely dictate their electrochemical performances due to the structural symmetry breaking from 3D (bulk) to 2D (surface), which leads to reconstructions under the different chemical/electrochemical conditions. By summarizing works in this subject and offering our perspectives, this tutorial review will reveal for the first time the correlation between surface structure and interface reconstruction at atomic/molecular scales and their direct impact on corresponding electrochemical performances. More importantly, by extending the knowledge obtained from these three well-studied system, we believe that the same priciples established could universally apply to other cathode materials that have been the frontiers of new battery chemistries.

Key Learning Points

1. Poorly crystalline and disordered surface can be reconstructed for higher capacities.
2. Electrolyte solvents are found to reconstruct the cathode/electrolyte interface, tuning the ion transfer kinetics.
3. The depolarization of cathode material can be achieved by a conductive coating layer in good contact with cathode surface.
4. Chemically and electrochemically stable phase or coating layer could be artificially applied on the particle in order to prevent surface degradation.

Introduction

In the efforts to improve lithium ion batteries (LIBs), a high-performance cathode material is often the key bottleneck. Among all reported cathode materials for LIBs, olivine-type $LiMPO_4$ (M = Fe, Mn, Co and Ni), layered lithium transition metal (TM) oxide $LiTMO_2$ (TM = Ni, Mn, Co or $Ni_xMn_yCo_z$, x+y+z = 1) and spinel $LiTM_2O_4$ (TM = Mn, Ti, Co or V) represent the three major groups of intercalation structures, and have been adopted in diversified electric vehicles (EVs) around the world. Olivine-type cathode material was first reported by Goodenough and co-workers in 1997.[1] Among these $LiFePO_4$ (LFP) is considered the most successful due to its moderate operating voltage (3.5 V vs Li/Li^+), moderate capacity, excellent environmental friendliness and low cost, high abundance of Fe, excellent stability and safety features. Layered lithium TM oxides present an alternative structure group to LFP with higher energy but lower safety and higher cost, whose application as automotive batteries is preferred given longer driving range. Spinel Li_2MnO_4 (LMO), with abundant annual global production capacity, is also regarded attractive owing to its low costs and good rate capability, although its cycling instability has been a persistent issue.

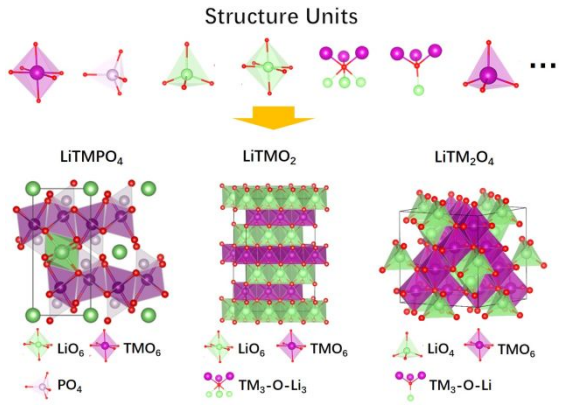

Figure 1. The major structural groups of cathode materials (olivine $LiTMPO_4$, layered $LiTMO_2$ and spinel $LiTM_2O_4$) in LIBs.

[a] School of Advanced Materials, Peking University Shenzhen Graduate School, Shenzhen 518055, China, Email: panfeng@pkusz.edu.cn
[b] Energy Storage Branch, Sensor and Electron Devices Directorate, Power and Energy Division, US Army Research Laboratory, Adelphi, MD 20783, USA
[c] Electrochemical Technology Program, Chemical Sciences and Engineering Division, Argonne National Laboratory, Illinois 60439, United States

Please do not adjust margins

Through periodic yet unique arrangement, basic structure units are able to constitute countless number of possible crystals.[2] These units can be considered as "material genes" that self-assemble into cathode materials, and they generally dictate charge transfer capability as well as structural stability of the eventual materials.[2] For instance, the olivine structure of LFP (**Figure 1**) consists of LiO_6 octahedra, FeO_6 octahedra and PO_4 tetrahedra, where Li-ion travels along the [010] direction. The strong covalent P-O bonding stabilizes O atoms and prevents oxygen release under oxidative conditions, thus making LFP a safe cathode material with excellent cycling stability.[3] In charged (delithiated) state, Li-ions are removed to form $FePO_4$ structure. This feature makes the lithiation/delithiation process of olivine LPF a two-phase transition reaction with a "transition zone" at the phase boundary, which differs from other cathode materials such as layered oxides. However, LFP exhibits relatively low electronic conductivity due to the covalent nature of its polyanions; meanwhile, the Li-Fe anti-site defects also result in poor percolation properties of Li^+ diffusion channel, leading to sluggish Li^+ diffusion.[4] Magnetic order around room temperature in Li_xFePO_4 ($x \leq 0.12$) was reported recently by Pan and co-workers,[5] who described that magnetism originated by Fe/Li antisite defects creates Fe^{2+}–Fe^{3+} superexchange to generate the strong Lorentz force tripping Li-ions, causing capacity loss. Other phosphates such as $LiTMPO_4$ (TM= Mn, Co or Ni) have also attracted researchers due to their higher voltage plateau (> 4 V vs Li/Li^+) compared with LFP. However, pristine $LiMnPO_4$ (LMP) suffers from the mismatched $LiMnPO_4/MnPO_4$ interface, even poorer electronic conductivity and the notorious Jahn-Teller distortion in charged state $MnPO_4$ which causes deformation of the MnO_6 octahedra and Mn dissolution and subsequent severe capacity fading. With much higher operating voltages, $LiNiPO_4$ (LNP, 5.1 V vs Li/Li^+) and $LiCoPO_4$ (LCP, 4.8 V vs Li/Li^+) were studied as potential high-energy-density alternatives, but their high operating voltages sets a barrier that no current electrolyte systems can overcome yet.

Adopting the classic α-$NaFeO_2$ type structure, layered TM oxides belong to a rhombohedral space group R $\bar{3}$ m with edge-sharing TMO_6 octahedra, and therefore exhibit alternating layers of Li^+ and TM ions bridged by oxygen atoms (Figure 1). Differing from LFP where Li-ion diffuses along a 1D channel, Li-slabs in TM oxide allow 2D diffusion of Li-ions from one LiO_6 octahedral site to another within the (001) plane. Instead of two phases like LFP, layered TM oxides exhibit single-phase solid solution during reversible lithiation/de-lithiation. More importantly, since Li-slabs and TM-slabs are merely connected by oxygen atoms, forming TM_3-O-Li_3 oxygen structure units, layered TM oxides are less stable than LFP. One major issue faced by layered TM oxides is the Ni/Li disordering, where Ni occupies 3b sites in Li-slab and Li occupies 3a sites in TM-slab due to the similar radii of Li^+ and Ni^{2+}. A high degree of Li/Ni disordering generally leads to poor specific capacity and cycle life. Furthermore, side reactions between layered TM oxides and electrolytes, surface phase transformation as well as particle cracking during repeated cycling could also contribute to the capacity fading.[6] In the recent years, Ni-rich layered oxides with high capacities have been intensively investigated, which are faced with not only more challenging storage and preparation issues, but also less stable surface due to high Ni content.[7]

The crystal structure of $LiMn_2O_4$ exhibits cubic spinel *Fd3m* space group with face-sharing 8a tetrahedral Li and 16d octahedral Mn (shown in Figure 1, right). During Li^+ insertion, additional Li-ions can be stored in 16c octahedral sites, which facilitate energetically accessible 3D interstitial pathways for Li^+ diffusion together with the 8a tetrahedral sites. The result of such structural nature is good rate capability for spinel LMO. However, LMO intrinsically suffers from poor cycling stability.[8] On one hand, discharge process induces Mn^{3+}-rich domain and causes Jahn-Teller distortion, further leading to Mn dissolution as well as blockage of Li diffusion pathway. On the other, Li insertion also results in phase transition from cubic $LiMn_2O_4$ to tetragonal $Li_2Mn_2O_4$ accompanied with large volume change and lattice mismatch, compromising the structural integrity.[8] In particular, LMO is especially susceptible to the attack of HF generated from water residue and $LiPF_6$ salt in the electrolyte, causing sustained surface degradation.

Although most efforts focused on their bulk properties, it is noteworthy that as the confined region for charge transfer process to occur, the interfacial structures cast a tremendous impact on the electrochemical properties (e.g. capacity, cycle life and high-rate performance) of battery materials. However, since the interface between the cathode and the electrode is an area of very limited presence, its chemical and electrochemical information is often obscured by the bulk. For instance, due to the disappearance of crystalline periodicity at the particle surface, the structural symmetry of cathode material is suddenly reduced from 3D to 2D, and such discontinuity usually presents high barriers to mobile ions. Owing to the development of advanced computational methods as well as surface characterization techniques, better understandings of surface structures, interface reconstruction and chemical properties in battery materials have been obtained in recent years. Kobayashi and co-workers used annular bright field (ABF) scanning transmission electron microscopy to examine the (010) surface of LFP.[9] As shown in **Figure 2A** and **Figure 2B**, they found that when the outer surface layer is shielded by Li atoms, P and Fe atoms has a larger vertical shift and larger distance; whereas when the surface Li site is vacant, P and Fe move towards each other. While after chemical delithiation, Li^+ are found to relax back to the bulk, the surface Li^+ cannot be recovered even after 3000 h of relaxation. Therefore, it could be inferred that the surface of olivine material may undergo structural reconstruction upon electrochemical processes. In addition, according to density function theory (DFT) calculations, migration process of Li^+ across LFP(010)/vacuum interface (**Figure 2C)** constitutes the limiting step due to the high migration energy.[10]

The surface structures of layered TM oxides also dictate their electrochemical performance. It has been reported by Kang and co-workers that when $LiNi_{0.5}Co_{0.2}Mn_{0.3}$ (NCM523) is cycled under a cut-off voltage of 4.5 V, the capacity retention is much higher than that cycled up to 4.8 V. This is because the surface of the particle undergoes a phase transformation from rhombohedral phase to spinel phase with a trace of rock salt phase NiO when cycled under 4.5 V (**Figure 2D**). Increasing the cut-off voltage to 4.8 V, the formation of rock salt phase is significantly accelerated under the

This journal is © The Royal Society of Chemistry 20xx

highly oxidative environment, accompanied by rapid capacity fading.[11] However, such transformation is not observed in $LiNi_{1/3}Co_{1/3}Mn_{1/3}$ (NCM111) material, which can be attributed to the lower content of Ni. In addition, the basic surface of NCM materials (especially for Ni-rich NMC) tends to react with CO_2 in the air, forming Li_2CO_3 on the surface. It has been reported that the impurities such as Li_2CO_3 could generate gas under high voltage, react with electrolyte and block Li^+ diffusion channels.[7]

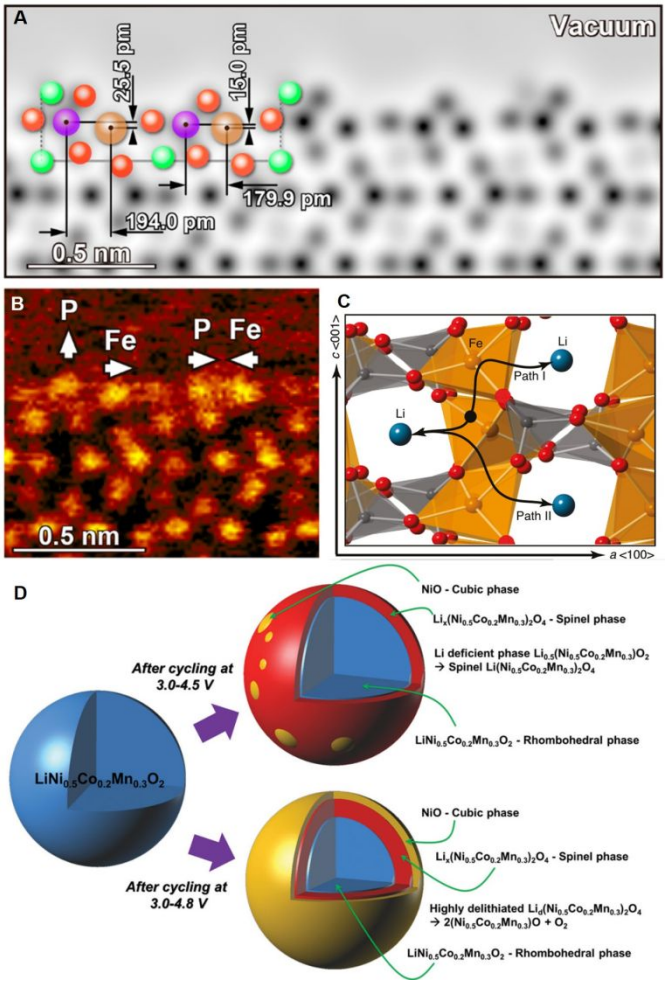

Figure 2. (A) Simulated annular bright field scanning transmission electron microscopy (ABF-STEM) image, where different atoms are colour-coded: Li-green, Fe-brown, P-purple, O-orange; (B) Magnified ABF-STEM colour images. The direction of atom shift is indicated by the white arrows. Reproduced from Ref. 9 with permission from American Chemical Society, copyright 2016. (C) Li^+ diffusion pathways on LFP surface. Reproduced from Ref. 10 with permission from American Chemical Society, copyright 2011. (D) Proposed transformation mechanisms of NCM532. Reproduced from Ref. 11 with permission from WILEY - VCH Verlag GmbH & Co. KGaA, Weinheim, copyright 2013.

Therefore, in order to optimize the electrochemical performance of cathode materials, a new interface is necessary through reconstruction reactions, which may vary with different chemical and electrochemical conditions. For instance, Ceder and co-workers reported that by forming a layer of fast ion-conducting amorphous phase on LFP through controlled off-stoichiometry preparation method, ultrafast charging and discharging performance can be achieved.[12] More importantly, due to the relatively lower operating voltages and robust crystalline structures, undesirable side reactions (e.g. Li/O release and electrolyte degradation) are less likely to occur on the LFP surface. Consequently, the surface of olivine and layered TM oxides represent two vastly different types of interfacial chemistry and electrochemistry.

In this tutorial review, as demonstrated in **Figure 3**, four types of interface reconstructions according to surface structures of different LIBs cathode materials will be summarized, which exhibit great relevance to the electrochemical performances including specific capacity, rate capability and cycling stability. By reviewing the recent advances in this area, we aim to clarify some fundamental questions about the interfaces of not only olivine, spinel and layered oxides, but also other cathode materials in general: how do mobile ions behave at the interface where structural discontinuity occurs? why is the interfacial structure so important to the bulk electrochemical performance? and how do we design to achieve a desirable interface?

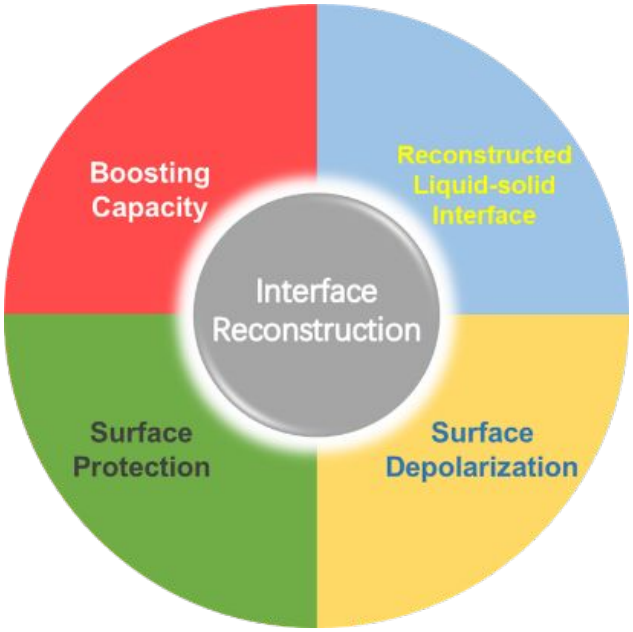

Figure 3. Diversified types of surface/interface reconstruction for olivine cathode materials.

Boosting Capacity *via* Surface Modification

The achievement of high-rate performance in LFP generally requires reduced particle sizes for shorter Li-ion diffusion path. However, this approach could compromise the overall energy density on device level by lowering the tap density. Moreover, the large surface area could also accelerate side reactions such as transition metal dissolution and electrolyte decomposition. In order to take full advantage of nanosized olivine materials, one effective strategy is to utilize their large specific surface areas by creating extra Li^+ storage sites on the particle surface. In 2013, Li and co-workers proposed LFP modified by exfoliated graphene (EG) *via* van der

Waals interaction,[13] which consists of a thin layer graphene (1.5-2 nm) coated on LFP particles. Consequently, a specific capacity of 208 mAh g^{-1} was achieved, which surpasses the theoretical value of LFP (170 mAh g^{-1}). More importantly, Li^+ insertion into EG was also observed after discharge. The authors hence attribute the excess capacity to the reversible redox-based Li^+ storage to the defects at edge sites or basal planes of the EG. In addition, the EG coating also promotes carrier mobility and reduces polarization.

Xiao and co-workers prepared a carbon encapsulated LFP (GC/LFP) with internal carbon (IC) sheet composite (GC/IC/LFP) using phytic acid.[14] Interestingly, both X-ray diffraction (XRD) and transmission electron microscope (TEM) results indicate that, compared with GC/LFP, GC/IC/LFP has a larger lattice parameter, which allows for faster Li^+ transfer. As a result, the obtained GC/IC/LFP exhibits a specific capacity of 192 mAh g^{-1}, which is also beyond the theoretical value of neat LFP. Both cyclic voltammogram and dQ/dV curves exhibit two redox peaks, suggesting that the excess capacity is related to an independent reversible redox reaction. It was speculated that the extra Li^+ might be stored both in the IC or its defects and edges. Alternatively, Sun and co-workers grew oxygen-containing functional groups (e.g. N-O· and C=O) on carbon surface coated on LFP, resulting in a capacity of 190 mAh g^{-1}.[15] They believed that these functional groups grafted on the carbon can be reversibly oxidized and reduced during charge and discharge processes, hence providing extra binding sites for Li^+.

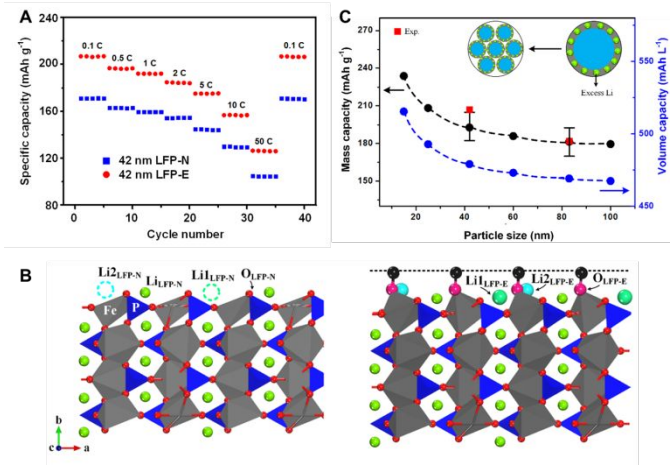

Figure 4. (A) Rate capabilities of LFP-N and LFP-E; (B) Lithium and electron transfer sites of excess Li atoms in LFP-N (left) and LFP-E (right); (C) Experimental and theoretical size-dependent excess capacity in LFP. Reproduced from Ref. 16 with permission from American Chemical Society, copyright 2017.

Despite the excitement about excess Li storage on the surface, the microscopic mechanisms of such behaviour remained unclear. To have a better understanding of their origin, Pan and co-workers investigated surface Li storage mechanism from the atomistic perspective.[16] By creating C-O-Fe bonds between the thin carbon coating layer and LFP, a new composite LFP-E was obtained, which also exhibited an ultra-high capacity of 208 mAh g^{-1} (**Figure 4A)**. Combining with ab initio calculations, it can be observed (**Figure 4B)** that due to the broken symmetry, Fe atoms on the surface of LFP are coordinated by 5 O atoms instead of 6, forming FeO_5 pentahedrons. This feature lowers the number of Li^+ storage sites on the surface by 50 %. By compensating the truncated symmetry of surface Fe atoms, the Fe-O-C bonds not only restored the original Li^+ storage sites, but also creates extra sites ($Li1_{LFP-E}$ and $Li2_{LFP-E}$) on the reconstructed surface by providing surface dangling O atoms which could bind with Li^+. It is noteworthy that the excess capacity is also size-dependent. **Figure 4C** summarizes the theoretical and experimental size-dependences of the specific capacity for LFP. Since smaller particles possess higher reconstructed surface areas and more excessive binding sites, higher capacity can be obtained thereon. In addition, this method was also effective on other olivine composites such as LMP, LCP, $LiFe_{0.5}Mn_{0.5}POI_4$ and $LiFe_{0.5}Co_{0.5}PO_4$. By modifying surface crystalline defects on olivine cathode materials, this approach opens up a new opportunity to higher capacities.[16]

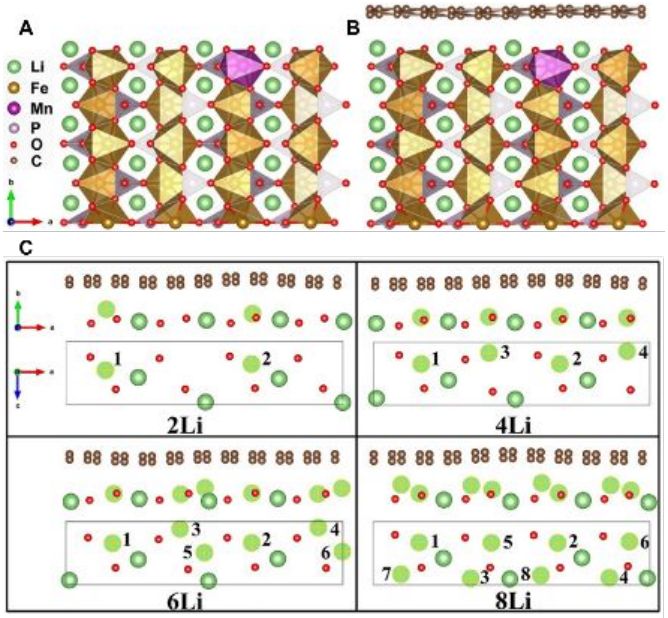

Figure 5. Side views of the structures of (A) LMFP surface and (B) graphene/LMFP interface. (C) Top and side views of the geometry optimized G/LFP interface with different numbers of Li atoms inserted. Only the outermost Li and O atomic layers are presented. Li atoms inserted are marked with yellow cross. Reproduced from Ref 17 with permission from Elsevier, copyright 2017.

Liu and co-workers also carried out first-principles total energy calculations on the Li insertion behaviour at the lithium manganese iron phosphate (LMFP)/graphene interface,[17] which allows the storage of 8 Li atoms with the insertion energy (E_{ins}) lower than 2 eV, corresponding to the lower cut-off voltage 2.0 V (**Figure 5**). According to this result, an excess capacity of 0.36 mAh cm^{-2} (per specific surface area of LFP particles) could be contributed by such interface, in agreement with the previous conclusion that the excess capacity is largely dependent on the particle size of olivine cathode material.

This journal is © The Royal Society of Chemistry 20xx

Please do not adjust margins

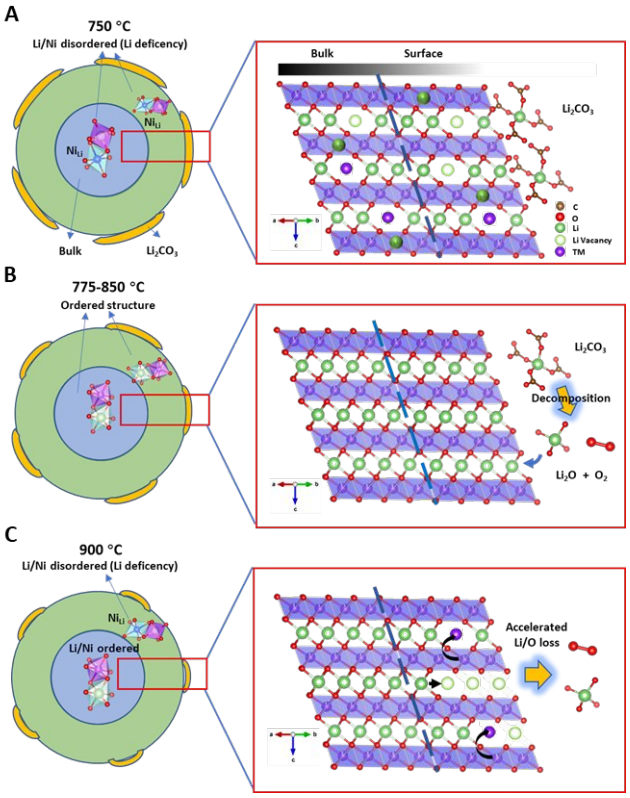

Figure 6. Schematic illustrations of how cationic ordering is coupled to surface reconstruction of NMC71515 under different sintering temperatures. Reproduced from Ref. 18 with permission from Royal Society of Chemistry, copyright 2019.

For lithium TM oxides, the more pressing issue is to suppress the formation of electrochemically inactive species on the surface. It is known that the sintering temperature of $LiNi_{0.7}Co_{0.15}Mn_{0.15}O_2$ (NCM71515) plays a critical role in its electrochemical performances.[18] On the one hand, when the temperature is too low, the Li_2CO_3 formed on the surface barely decompose, leading to Li-deficient particle surface with a passivation layer, hence the low capacity (**Figure 6**). On the other, if the temperature is too high, while sufficient for the structural ordering process, the rate of Li/O loss at the surface is promoted, leading to a Li-deficient phase near the particle surface. Therefore, by choosing an optimized temperature window, desirable surface reconstruction (Li_2CO_3 decomposition) could be favoured while unwanted Li/O loss circumvented. More recently, it is also found that the cooling-induced surface reconstruction has a pronounced effect on the capacity as well as rate capability.[19] By adopting a quenching process, the accumulation of Li_2CO_3 on the surface is suppressed, hence the Li-deficient phase on the surface can be effectively avoided.

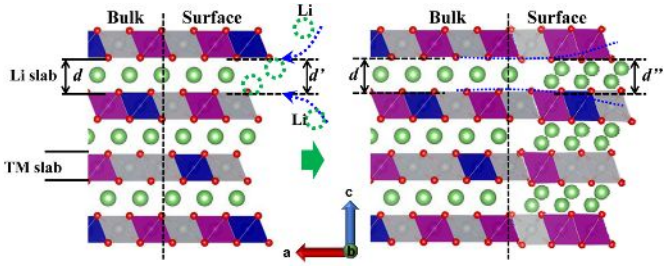

Figure 7. Schematic mechanisms of the prelithiation process for NCM523. Reproduced from Ref. 20 with permission from American Chemical Society, copyright 2015.

Pan and co-workers proposed a prelithiation process to improve the capacity and cycling stability of $LiNi_{0.5}Co_{0.2}Mn_{0.3}O_2$ (NCM523) material by treating the active material at low voltage (1.2 V vs Li/Li^+) before cycling.[20] As a result, an SEI from electrolyte reduction can be formed on the particle surface of NCM523, which prevents Mn^{2+} dissolution during the subsequent cycling in normal voltage ranges. More importantly, an additional layer of Li^+ can be reversibly stored in the surface, contributing to a higher capacity (**Figure 7**).

Reconstructing Liquid-Solid Interface

Diffusion of Li^+ across the interface is more sluggish than in bulk, hence approach to accelerate this process is of high significance. According to Bazant and co-workers, ab initio molecular dynamics (MD) simulations show that the Li^+ transfer between LFP (010) face and vacuum is inhibited due to the high diffusion energy.[21] The presence of both organic and aqueous solvent molecules are found to assist this surface diffusion, rendering LFP a 3D Li^+ conductor (**Figure 8**). Therefore, understanding the Li^+ migration mechanism at the interface between olivine materials and electrolyte in molecular/atomic scales becomes critical for material designing and developing.

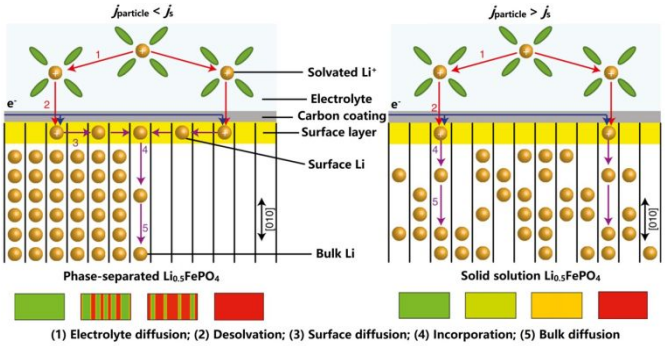

Figure 8. Different Li^+ diffusion mechanisms during phase separation (left) and solid solution reaction (right). Reproduced from Ref. 21 with permission from Nature Publishing Group, copyright 2018.

In recent years, aqueous electrolytes have attracted extensive interests due to their intrinsic safety and lower costs than conventional non-aqueous electrolytes. Due to the relatively low operation potential of LFP, aqueous electrolyte could stably support such cathode without generating oxygen at its anodic limits. Using

nanosized LFP as cathode material, Pan and co-workers compared electrochemical performance of an aqueous electrolyte with 0.5 M Li_2SO_4 with conventional carbonate electrolyte.[22] The water-based electrolyte exhibited ultrafast rate capability (72 mAh g^{-1} at 600 C, corresponding to 42% charge completed at 6 seconds), which is much higher than the carbonate (20 mAh g^{-1} @ 200 C). Using DFT simulation, it is proposed that this difference originated from an "Janus interface" facilitated by H_2O molecules. The FeO_6 and LiO_6 octahedral structure units in crystal experience a symmetry breaking to become FeO_5 and LiO_3 units at the surface, (**Figure 9A**) which can be compensated by O atoms from H_2O, forming $FeO_5(H_2O)$ and $LiO_3(H_2O)_3$ octahedra; meanwhile, H atoms could also form strong hydrogen bonds with adjacent O atoms to widen the Li^+ passage by approximately 0.2 Å for faster Li^+ (de)intercalation. Consequently, a transition structure that resembles both solid and liquid phases is formed, which serves as the optimum transition phase for fast Li^+ transfer. In addition, for aqueous electrolyte, the overall energy barrier of de-solvation process is much lower than that in organic electrolyte due to fewer number of H_2O molecules are involved (**Figure 9B** and **9C**).

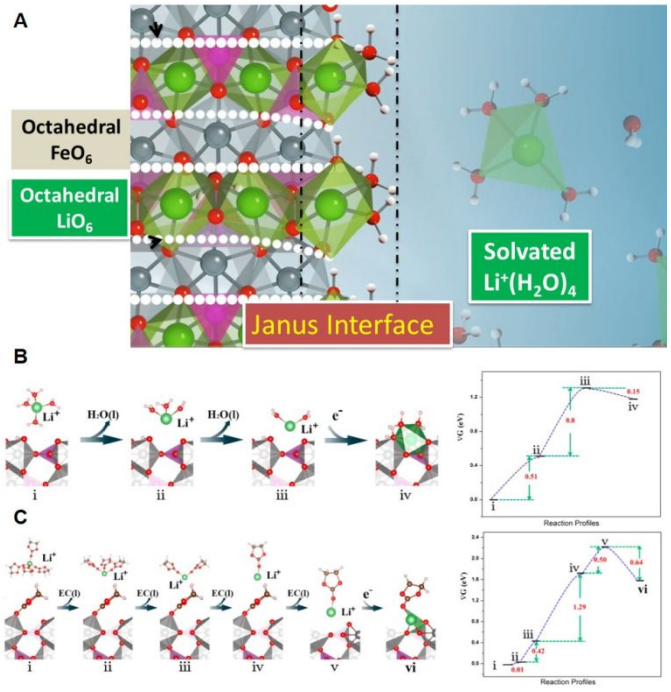

Figure 9. (A) Proposed Janus solid-liquid interface between LFP and aqueous electrolyte; Reaction profiles for Li-ions transport across the $FePO_4/H_2O$ interface (B) and $FePO_4$/ethylene carbonate (EC) interface (C) in the discharge process and their energies at each step (right-hand panels). Li, green; Fe, grey; P, purple; O, red; C, brown; H, white. Reproduced from Ref. 22 with permission from American Chemical Society, copyright 2015.

To further understand the underlying mechanisms, advanced electrochemical characterization techniques have been tailor-developed and employed. For instance, by using electrochemical quartz crystal microbalance (EQCM), Pan and co-workers measured the mass changes of LFP and NFP cathode during electrochemical processes.[23] In organic electrolyte, LFP exhibits conventional Li^+ (de)intercalation processes as expected (**Figure 10A**); however, in aqueous electrolyte, the mass curve shows an increase trend at 3.42-3.44 V vs Li/Li^+ even during charging, and similar anomalous mass change interval can also be observed during cathodic scanning. The mass-charge curve obtained from aqueous solution shows a higher value of 11 g mol^{-1} compared to that in organic electrolyte (approximately 7 g mol^{-1}, equivalent to the mass/charge ratio of a Li^+). The intercalation/deintercalation processes can be divided into two stages (**Figure 10B**): during the surface redox process, H_2O molecules are desorbed with surface Li^+ when the potential reaches the de-lithiation "surface potential" (V_{surf}), at which the bulk Li^+ have insufficient driving force to migrate into surface layers due to that V_{surf}(2.9V) < V_{bulk}(3.4V) according to DFT calculation. Then H_2O molecules are re-adsorbed on Li^+ of the LFP surface once the potential is aroused to V_{bulk}, whereas during the bulk redox process, the surface reaction reaches a dynamic equilibrium, leading to a continuous mass change. By contrast, such behaviour cannot be observed in an aqueous NFP cell, which can be ascribed to the fact that the surface and bulk redox voltages are too close to distinguish under the condition of the cyclic voltammetry (CV) measurement. Interestingly, it has also been reported that different from non-aqueous electrolyte, Na^+ can be preferentially inserted into $FePO_4$ framework over Li^+ in aqueous solution due to the lower energy barrier at the $FePO_4/H_2O$ interface.[24] Taking advantage of this feature, NFP with good electrochemical performance can be synthesized via a facile ion-exchange process.

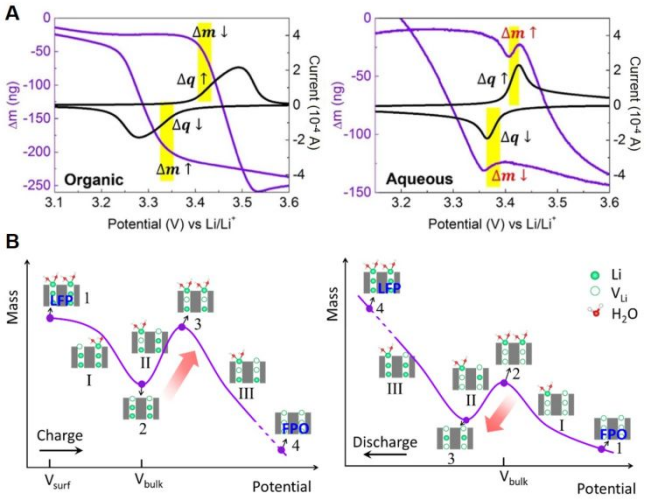

Figure 10. (A) Mass-potential curves (purple line) and CV curves (black line) of LFP in organic electrolyte (left) and aqueous electrolyte (right); (B) Proposed mass-potential curves for $LiFePO_4$ in aqueous system during charge (left) and discharge (right). Reproduced from Ref. 23 with permission from Elsevier, copyright 2017.

Thick electrodes with high areal loading and particle aggregation are favoured inconsideration of high energy densities. As a result, too much information (e.g. particle-particle interaction, pore-accessibility by electrolyte and concentration polarization within electrolyte) is entangled in the electrochemical data obtained, which cannot reflect the intrinsic properties of individual single particles. In

This journal is © The Royal Society of Chemistry 20xx

Please do not adjust margins

addition, galvanostatic intermittent titration technique (GITT) is not suitable for LFP due to its flat voltage plateaus. To exclude those interfering factors and to obtain electrochemical information of single LFP particles, Pan and co-workers fabricated an ultrathin single-particle (SP) electrode,[25] where LFP nanoparticles were uniformly scattered within the conductive network. Compared with conventionally prepared electrode (thick electrode), the anodic peak in SP electrode shows a much narrower half-width (**Figure 11A**), indicating minimized polarization effect. A novel SP Model was then developed to fit the CV curves of SP electrodes, which include Li^+ diffusion process and interface charge transfer process to obtain parameters of Li^+ diffusion coefficients (D_{Li}) and interface reaction rate constants (K_0). It can be seen from **Figure 11B** that the CV curves of SP electrodes in both water-based and carbonate electrolytes can be well fitted by the model. The fitted K^0 in aqueous electrolyte is higher than that in organic electrolyte by one order of magnitude. Here the K^0 value is associated with the pre-exponential factor(A) and activation energy (E_a) ($\ln K_0 = \ln A - E_a/RT$; R: molar gas constant; T: thermodynamic temperature), while A and E_a can be attributed to the de-solvation (solvation) process and interface reconstruction with solvent (e.g. H_2O-Fe coordination), respectively (presented as Step II in **Figure 11C**). This result agrees with the previous conclusion that the de-solvation process is the determining step for the Li-ion transport across $FePO_4$/electrolyte interface. Recently, the effect of anion adsorption layer in inner Helmholtz plane is also investigated. It is revealed that different anions exhibit different binding energy with LFP surface, resulting in a significant impact on K_0 and E_a.[26]

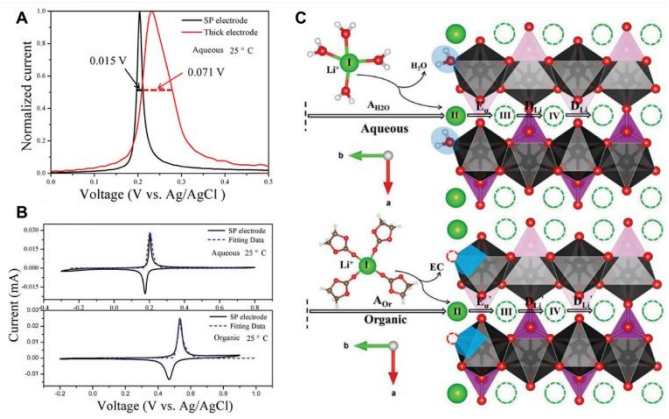

Figure 11. (A) CV curves of SP and thick electrodes; (B) CV curves of SP electrode and thick electrode in aqueous and organic electrolyte at 25 °C with the current density of 1 mV s^{-1}, the dotted lines are the simulation curves by the SP-model; (C) The interfacial reaction profiles for Li-ions transport across the $FePO_4/H_2O$ interface and $FePO_4$/EC interface in the discharge process. Reproduced from Ref. 25 with permission from WILEY - VCH Verlag GmbH & Co. KGaA, Weinheim, copyright 2016.

Surface doping is also found to have significant impact on reconstructing the solid-liquid interface. Chen's group reported that by doping a small amount of Ni on the surface of LMO, the capacity and rate performance of LMO is greatly promoted at -20 °C.[27] Through DFT calculations, it is revealed that the reconstructed interface demonstrates a significantly reduced energy barrier for charge transfer and Li binding energy. Therefore, the synergistic effect in the outmost layers lowers the threshold energy of the interfacial reactions. It should be noted that owing to the unstable electrode-electrolyte interface during cycling, it is much more difficult to obtain detailed interfacial information of spinels and layer oxides. For future studies, one key challenge is to optimize the testing conditions.

Depolarizing Cathode Materials and Electrodes

The slow Li^+ diffusion and poor intrinsic electronic conductivity have imposed severe restrictions on the rate performances of cathode materials, therefore, several measures have been adopted to address this issue. The surface/interface depolarization of cathode materials can be carried out by either improving the ionic or the electronic conductivities. With the aid of a statistical method of Tafel analysis, Bai and Bazant reveal that the electron transfer at solid-solid interface constitutes the limiting step for reaction kinetics of LFP rather than the ion transfer at the liquid-solid interface.[28]

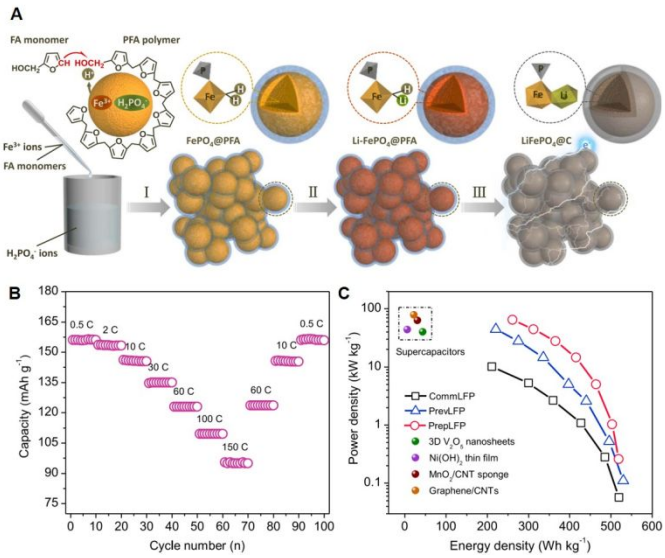

Figure 12. (A) Schematic illustration for the preparation process of LFP/C material; (B) Rate performance and (C) Ragone plot of power density versus energy density of LFP/C nanocomposite. Reproduced from Ref. 29 with permission from Elsevier, copyright 2017.

The most commonly used strategy for higher electronic conductivity is to coat a thin layer of conductive materials (e.g. carbon) on the surface of olivine materials. Generally, the carbon coating process involves pyrolysis of organic precursors at reducing atmosphere. As shown in **Figure 12A**, a LFP/C nanocomposite material is synthesized by a self-regulated in-situ polymerization method (Step I), followed by a rapid Li^+/H^+ ion exchange step (Step II) and calcination (Step III).[29] On one hand, LFP/C particles with highly crystalline LFP cores was obtained; on the other, highly graphitized carbon were formed on LFP surface due to the catalytic effect of Fe^{3+}. This ideal feature can be attributed to the hybrid structure of Li-$FePO_4$/PFA intermediate with a well-closed polymer "shell" and a homogeneous "core" where essential elements are

homogeneously distributed at atomic level. This LFP/C composite obtained from such method (PrepLFP) exhibits superior rate capacity (**Figure 12B**) as well as power/energy density (**Figure 12C**) compared with other battery/supercapacitor materials.

The choice of conductive additive also determines the electronic conductivity. Pan and co-workers compared the effect of carbon with different contacting properties on the performance of LFP cathodes.[30] They found that soft-contact carbon (SCC) with less crystalline structure enables better electronic conduction as compared with hard-contact carbon (HCC), thus leading to superior rate capability. SCC induces plane-like contact with large area rather than the point-like contact generated by HCC according to the simulation (**Figure 13**). More uniform current density vectors are expected for the interface between LFP and SCC, hence the alleviated polarization effect.

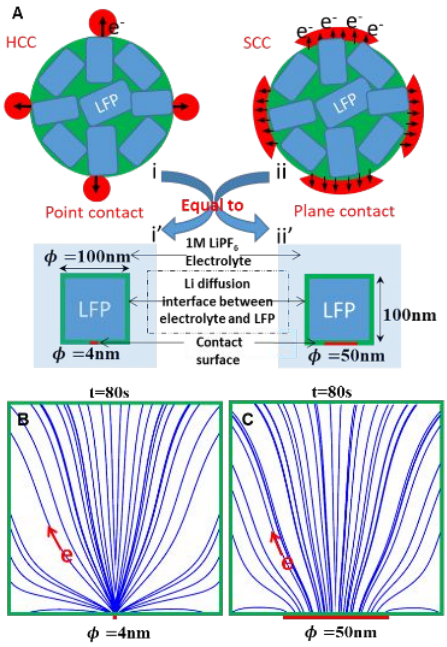

Figure 13. (A) Schematic illustration of different contact types of LFP with HCC and SCC; Simulated current density vectors within LFP for electrodes with (B) HCC and (C) SCC. Reproduced from Ref. 30 with permission from Elsevier, copyright 2016.

However, it should be cautioned that the carbon coating could cause non-stoichiometric composition on LFP surfaces, leading to unwanted capacity loss. It has been reported by Sun and co-workers that during the carbon-coating process, electrochemically inert phases (Fe_2P and $Fe_2P_2O_7$) emerge on the surface due to lithium loss during thermal treatment. Moreover, the formation of these impurity phases is highly dependent on particle size, sintering temperatures and atmosphere.[31] Therefore, conductive polymers are also considered as promising coating materials for olivine cathode materials due to the environmental friendliness and low energy costs. *Via* the polymerization of 3,4-ethylenedioxythiophene (EDOT), Lepage et al. coated LFP particles with a thin layer of poly(3,4-ethylenedioxythiophene) (PEDOT),[32] which resulted in excellent rate performance comparable to that of the carbon-coated materials. Alternatively, Peng and co-workers proposed a conducting polymer coating of polyphenylene that binds with micron-sized LFP particles (about 1.01 μm) *via* a green diazonium chemistry (**Figure 14A**),[33] in which diazonium cations are first chemically reduced to phenyl radicals by LFP. DFT simulation results have shown that phenyl radicals could form strong chemical bond with O sites on a Li-deficient surface (**Figure 14B-D**), which allows intimate binding between LFP and the conductive polymer. As a result, micron-sized LFP materials with improved electronic conductivity can be obtained, exhibiting excellent electrochemical performance.

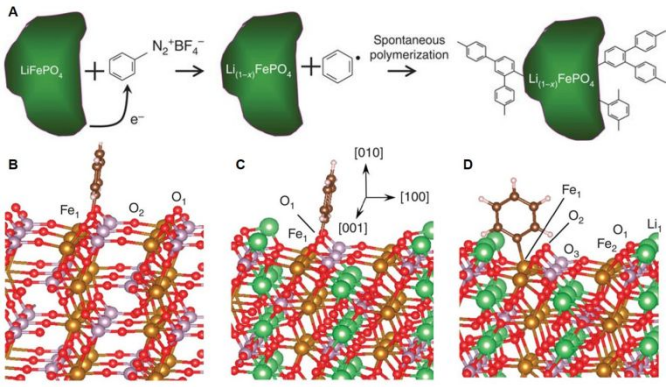

Figure 14. (A) Schematic illustration of the polymerization reaction; DFT calculated configurations of phenyl radical on (010) face for (B) $FePO_4$, (C) LFP with Li vacancy and (D) stoichiometric LFP. Reproduced from Ref. 33 with permission from Nature Publishing Group, copyright 2015.

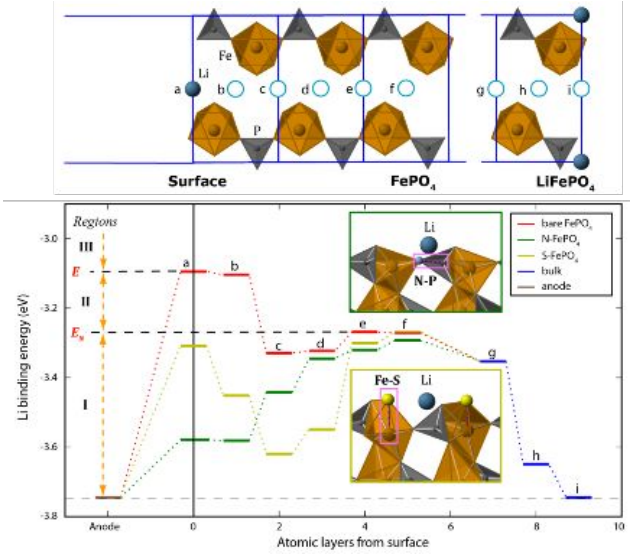

Figure 15. Energy landscapes of Li moving through the surface of bare $FePO_4$ and doped $FePO_4$. Reproduced from Ref. 34 with permission from American Chemical Society, copyright 2012.

The depolarization can be also achieved by surface doping. Goodenough and co-workers have reported that through doping nitrogen and sulphur on the surface of LFP, the rate capability can be greatly improved.[34] The calculation results show that nitrogen preferably substitutes for oxygen in the PO_4 tetrahedral and sulphur

This journal is © The Royal Society of Chemistry 20xx

Please do not adjust margins

bonds to undercoordinated Fe atoms on the surface (**Figure 15**). As a result, the broken symmetry on the LFP surface is compensated. From the calculated binding energy of a Li^+ as it diffuses from (010) surface to different atom layers during discharge process, it can be observed that on bare LFP, Li^+ binds weakly at subsurface sites (a and b) owing to the undercoordinated surface. This binding become stronger as Li^+ reaches the bulk. The doping of N and S could effectively tune the energy levels on the surface by providing an empty state in the band gap and stabilizing the surface Fe 3d antibonding states, respectively, resulting in lower diffusion barriers for Li^+ diffusion. Alternatively, 1% Zr doping in Li-excess LFP ($L_{1.035}Zr_{0.01}FP$) is found to form a highly conductive layer on the surface,[35] which works synergistically with carbon layer to enhance the conductivity. Consequently, improved rate performance was obtained. However, it should be noted that excessive doping (2% of Zr) inflict a detrimental effect on the electrochemical performance due to the compromised LFP crystalline structures.

Since the carbon-coating technique requires reducing atmosphere, which cannot be applied to layered lithium TM oxides, building an electronic conductive network in such system is more challenging. In order to address this issue, Pan and co-workers proposed a new concept of material design by embedding NCM523 particles in the single-wall carbon nanotube (CNT) network (**Figure 16A**).[36] From **Figure 16B**, it can be observed that the cathode particles are homogeneously wrapped by CNTs, which serve as a highway for the electron transfer, leading to a reduced electronic resistivity. As a result, the CV curve (**Figure 16C**) of NCM523/CNT composite shows sharp peak indicative of fast kinetics.

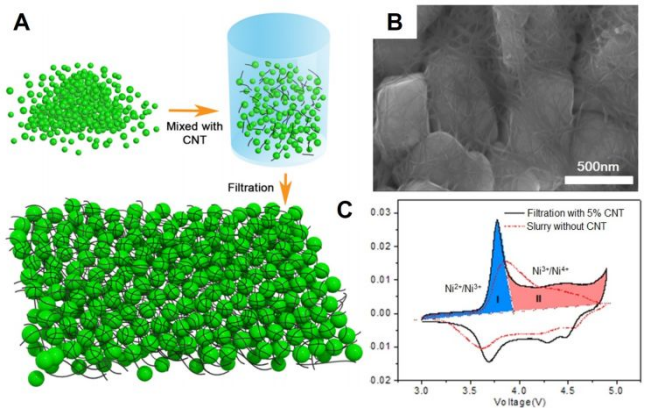

Figure 16. (A) The schematic of the preparation process for the NCM/CNT film cathode; (B) Scanning electron microscope (SEM) image of NCM/CNT cathode composite; (C) CV curve comparison for the slurry NCM without (dash line) and filtration NCM with CNT (solid line) cathodes. The two delithiation stages in the filtration NCM cathode are coloured in blue (I, Ni^{2+}/Ni^{3+}) and pink (II, Ni^{3+}/Ni^{4+}). Reproduced from Ref. 36 with permission from American Chemical Society, copyright 2014.

Surface Protection of Cathode Materials

Aurbach and co-workers proposed that the formation of trace HF, which is inevitable in the commonly used $LiPF_6$-based electrolyte, accelerates the failure of LFP cathode:[37] on one hand, Fe-ion experiences ion- exchange with H^+, causing Fe dissolution as well as capacity fading; on the other, Li^+ combines with F^-, forming highly resistive LiF, which slows down the charge transfer kinetics. Sun and co-workers later carried out visual observation of surface corrosion of LFP, where two types of impurity phases are identified: Fe-rich and P-rich phases.[38] It is found that severe Fe dissolution occurs in Fe-rich phase due to the lower corrosion potential, which inhibits the corrosion of the adjacent area. On the contrary, P-rich phase is more stable due to its high corrosion potential, which promotes the corrosion of the adjacent area. Despite these studies regarding surface degradation mechanisms of LFP, its surface protection strategy has not been not considered a priority owing to its excellent cycling stability.

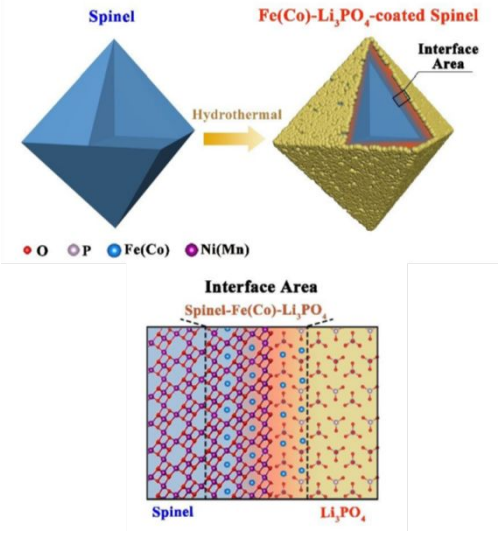

Figure 17. Scheme of the phosphate coating mechanism of spinel cathode materials. The Fe and Co ions in the starting solution will migrate into the 16c sites of the spinel surface to form a bridge layer at the interface between spinel and $LiPO_4$, facilitating a dense and uniform Li_3PO_4 coating layer. Reproduced from Ref. 41 with permission from American Chemical Society, copyright 2019.

Mn dissolution in LMP (same applies to LMO) is believed to have undergone a similar route, where the surface Mn is attacked by the trace HF in the fluorine-containing electrolyte. However, the Mn dissolution is much more severe due to the instability of Mn^{3+}. More importantly, the dissolved Mn species are found to deposit on the anode (e.g. graphite), causing further deterioration of SEI, consuming Li^+, and consequently resulting in faster capacity fading.[39,40] Therefore, for commercialization of Mn-doped olivine cathode materials, it is of great importance to suppress the dissolution of Mn species. It is increasingly clear and widely demonstrated that one of the most effective strategies is to apply a coating layer to stabilize the surface. In this case, how well-bonded the interface is between the coating layer and the cathode surface should be also taken into considerations. Huang and co-workers reported that by adding a small amount of bridging ions (e.g. Fe and Co) upon coating process, strong bonding between spinel and the coating agent (i.e. Li_3PO_4) can be achieved.[41] They found that Fe and Co will diffuse into both the

16c sites to form a reconstructed interface (spinel-Fe(Co)-Li_3PO_4), which allows facile and homogeneous coating (**Figure 17**). By contrast, in the absence of bridging agents, the same procedure results no Li_3PO_4 coating layer on the surface.

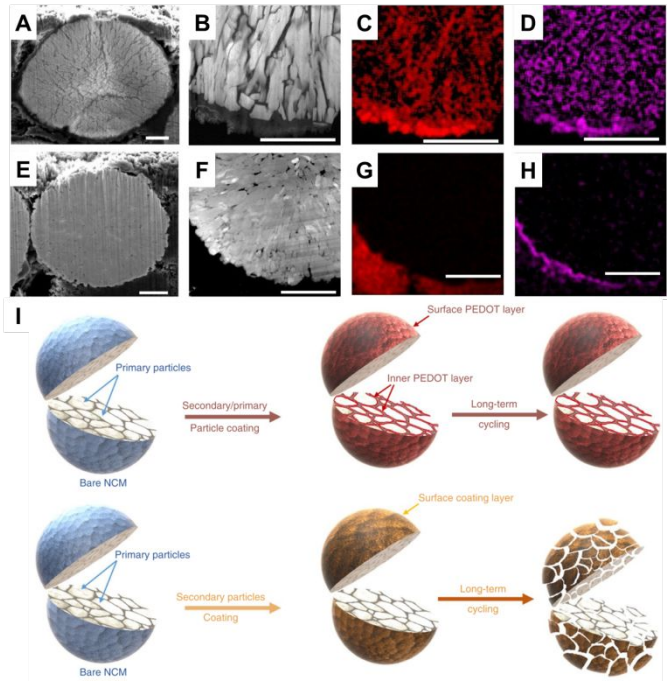

Figure 18. Cross-sectional SEM image (A), scanning transmission electron microscope high-angle annular dark field (STEM-HAADF) image (B) and the corresponding C (C) and F (D) maps of pristine electrode after 200 cycles; Cross-sectional SEM image (E) STEM-HAADF image (F) and the corresponding C (G) and F (H) maps of LPO-infused electrode material after 200 cycles. Scale bars, 2 µm. Reproduced from Ref. 42 with permission from Nature Publishing Group, copyright 2018. (I) An illustration of the structural stability of both secondary/primary particle coating and secondary particle coating only after long-term cycling. Reproduced from Ref. 43 with permission from Nature Publishing Group, copyright 2019.

For layered oxides, especially Ni-rich materials, side reactions on the liquid-solid interface could also lead to phase transition, hence the intergranular cracking. Electrolyte will then further infiltrate into the grain boundaries to react with cathode materials. Therefore, a protective buffer layer could be an effective to stabilize the particle surface. *Via* ALD technique, Yan et al. infused a solid electrolyte, Li_3PO_4 (LPO) into the grain boundaries of Ni-rich layered oxide $LiNi_{0.76}Co_{0.14}Mn_{0.1}O_2$ material.[42] The LPO not only provides Li^+ diffusion pathways between grain boundaries, but also solidifies the grain boundaries of $LiNi_{0.76}Co_{0.14}Mn_{0.1}O_2$. As a result, compared with pristine material, where severe intergranular cracking occurs during continuous cycling (**Figure 18A** to **18D**), the permeation of liquid electrolyte is minimized by the LPO coating layer, suppressing the formation of spinel-phase surface. As a result, the cracking is effectively prevented (**Figure 18E** to **18H**), hence the better electrochemical performances.

More recently, using oxidative chemical vapour deposition technique, Amine and co-workers applied a conformal coating of conductive polymer poly(3,4-ethylenedioxythiophene) (PEDOT) on both primary and secondary particles of layered oxide materials as the protective skin (**Figure 18I**).[43] During long-term cycling, the PEDOT coating greatly enhances the phase and morphology stability of layered oxides, exhibiting much higher capacity retention compared with bare particles. In addition, the PEDOT layer serves as an HF-scavenging agent by forming O-H-F bonds. As a result, the overall concentration of HF is decreased by 50% and the TM dissolution is significantly inhibited, hence the better cycle stability.

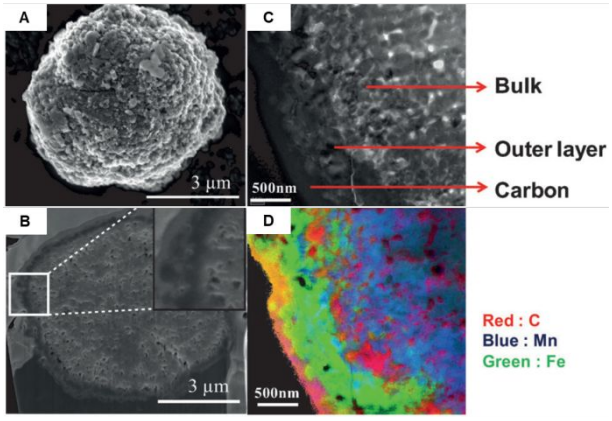

Figure 19. SEM images of (A) double-structured $LiMn_{0.85}Fe_{0.15}PO_4$–LFP and (B) its cross-sectional image; (C) Magnified cross-sectional TEM image and (D) its corresponding electron energy loss spectroscopy (EELS) image. Reproduced from Ref. 48 with permission from WILEY - VCH Verlag GmbH & Co. KGaA, Weinheim, copyright 2012.

Alternative approach to avoid the side reactions at the electrode/electrolyte interface is through surface enrichment of certain stable component. Liu and co-workers have developed a concentration-gradient $LiMn_{0.8}Fe_{0.2}PO_4$ material (CG-LMFP).[44] Both X-ray photoelectron spectroscopy (XPS) and energy dispersive X-ray spectroscopy (EDXS) mapping analysis results have confirmed that CG-LMFP has a Fe-rich surface and Mn-rich core. The obtained product shows remarkably enhanced stability against HF attack and effectively suppresses Mn dissolution. Superior cycling capacity and stability were achieved compared to pristine LMFP. Since lithium TM oxides (especially those rich in Ni) suffer from severe side reactions with electrolyte at high voltages due to the instability of Ni^{4+}, diluting Ni concentration on the surface is considered an effective method. Sun and Amine designed a $LiNi_{0.75}Co_{0.1}Mn_{0.15}O_2$ with concentration-gradient nanostructures (Ni-rich core and Mn-rich surface).[45] The concentration of Co and Ni decreases linearly from the centre to the surface whereas Mn is enriched on the surface. This concentration-gradient material shows not only longer cycling life, but also improved thermal stability. A Ti gradient doped (Ti/TM = 1.6%) $LiNi_{0.8}Co_{0.2}O_2$ (NC82) with high Ti concentration on the surface was developed by Pan and co-workers recently. Consequently, an electrochemically favoured disordered layered phase is formed at the surface, leading to a greatly improved cycling stability and superior rate capability. First-principles calculations further reveal that the excellent electrochemical performance is attributed to the robustness of the oxygen-framework after Ti doping.[46] Similarly, Hu

This journal is © The Royal Society of Chemistry 20xx

and co-workers synthesized pherical concentration-gradient $LiMn_{1.87}Ni_{0.13}O_4$, where the outmost layer is $LiMn_{1.5}Ni0_{0.5}O_4$ and the core is pure LMO.[47] Compared with prestine LMO, the concentration-gradient material delivers a much longer cycle life at elevated temperature (55 ℃) as well as high operating voltage (3.0 – 4.9 V vs Li/Li^+).

Alternatively, Oh et al. synthesized micron-sized $LiMn_{0.85}Fe_{0.15}PO_4$ coated with a layer of LFP with thickness of 0.5 μm (**Figure 19**).[48] This material not only adopts the high volumetric energy density of LMFP, but also exhibits improved rate capability and cycling stability of LFP located at its outer layer. The similar strategy was applied to $LiCoPO_4$ (LCP), which suffers from even more severe surface degradation owing to its high operation potential (~4.7 V). A robust monolithic LFP coat layer was hence formed by Manthiram and co-workers on high voltage vanadium-substituted LCP ($LiCo_{1-3x/2}V_x\square_{x/2}PO_4$) using microwave-assisted solvothermal approach.[49] Such LFP-coated LCP material exhibits lowered voltage polarization as well as required charge potentials. A coulombic efficiency of 100% can be achieved at x = 0.04, indicating mitigated surface side reactions. This surface protection approach can be universally applied on other materials. Through an elegant atomic-level engineering, Pan and co-workers managed to design and synthesize a a core-shell NCM@LFP material with aligned Li^+ tunnels, the result of which is the improved cycling stability of layered oxide materials at 4.6 V vs Li/Li^+.[50]

Conclusions

The recent advances in developing and understanding intercalation cathode materials revealed the essential but overlooked role of interfacial structure and chemistry in determining the electrochemistry of these materials. As the legitimate region for charge transfer to occur, the discontinuity, the truncated symmetry and the concomitant impurity phases all affect the kinetics and thermodynamics of the ion transport. By summarizing these studies, we aim to gain a better understanding about how to manipulate this key component at the atomic scale. It is noteworthy that due to different structure units and their arrangements, operating voltages and electrolyte systems, desirable interfaces and the corresponding surface engineering could vary remarkably from material to material. However, they are expected to share similar chemical/electrochemical properties such as high stability and fast charge transfer capability. Herein, several key conclusions have been made as follow, which may provide solutions to improve not only olivine, spinel and layered oxides, but in broader term all intercalation host materials:

a. Through surface modification, the poorly crystalline or disordered surface of cathode materials can be utilized for additional Li^+ binding sites, providing higher capacities;
b. The ion transfer kinetics across the cathode/electrolyte interface can be tuned by choosing alternative solvents or surface doping, which could reconstruct the truncated surface symmetry and lower the migration energy barrier as well as the de-solvation energy, enabling better rate performance;
c. To improve the rate capability of materials with poor electronic conductivity, surface depolarization of cathode material can be achieved by a conductive coating layer (e.g. carbon or conductive polymer), which is preferably in close (e.g. molecular level) contact with the cathode surface;
d. In order to stabilize the cycling performance of cathode materials which are prone to surface degradation, chemically and electrochemically stable phase or coating layer could be introduced to the outer layer of the particle.

Conflicts of interest

There are no conflicts to declare.

Acknowledgements

This work is supported by National Key R&D Program of China (2016YFB0700600), National Natural Science Foundation of China (No.51672012), Guangdong Key-lab Project (No. 2017B0303010130), and Shenzhen Science and Technology Research Grant (ZDSYS20170728102618). KX also wants to thank the Joint Center for Energy Storage Research, an Energy Innovation Hub funded by the U.S. Department of Energy, Office of Science, Basic Energy Sciences through IAA SN2020957.

Notes and references

1 A. K. Padhi, K. S. Nanjundaswamy and J. B. Goodenough, *J. Electrochem. Soc.*, 1997, **144**, 1188–1194.
2 J. Zheng, Y. Ye and F. Pan, *Natl. Sci. Rev.*, 2019, nwz178.
3 X. Liu, Y. J. Wang, B. Barbiellini, H. Hafiz, S. Basak, J. Liu, T. Richardson, G. Shu, F. Chou, T. C. Weng, D. Nordlund, D. Sokaras, B. Moritz, T. P. Devereaux, R. Qiao, Y. De Chuang, A. Bansil, Z. Hussain and W. Yang, *Phys. Chem. Chem. Phys.*, 2015, **17**, 26369–26377.
4 J. Lu, Z. Chen, F. Pan, L. A. Curtiss and K. Amine, *Nat. Nanotechnol.*, 2016, **11**, 1031–1038.
5 J. Hu, H. Zeng, X. Chen, Z. Wang, H. Wang, R. Wang, L. Wu, Q. Huang, L. Kong, J. Zheng, Y. Xiao, W. Zhang and F. Pan, *J. Phys. Chem. Lett.*, 2019, 4794–4799.
6 J. Zheng, Y. Ye, T. Liu, Y. Xiao, C. Wang, F. Wang and F. Pan, *Acc. Chem. Res.*, 2019, **52**, 2201–2209.
7 B. Xiao and X. Sun, *Adv. Energy Mater.*, 2018, **8**, 1802057.
8 G. Xu, Z. Liu, C. Zhang, G. Cui and L. Chen, *J. Mater. Chem. A*, 2015, **3**, 4092–4123.
9 S. Kobayashi, C. A. J. Fisher, T. Kato, Y. Ukyo, T. Hirayama and Y. Ikuhara, *Nano Lett.*, 2016, **16**, 5409–5414.
10 G. K. P. Dathar, D. Sheppard, K. J. Stevenson and G. Henkelman, *Chem. Mater.*, 2011, **23**, 4032–4037.
11 S. K. Jung, H. Gwon, J. Hong, K. Y. Park, D. H. Seo, H. Kim, J. Hyun, W. Yang and K. Kang, *Adv. Energy Mater.*, 2014, **4**, 1300787.
12 B. Kang and G. Ceder, *Nature*, 2009, **458**, 190.
13 B. Lung-Hao Hu, F. Y. Wu, C. Te Lin, A. N. Khlobystov and L. J. Li, *Nat. Commun.*, 2013, **4**, 1687.

14 Q. Zhao, Y. Zhang, Y. Meng, Y. Wang, J. Ou, Y. Guo and D. Xiao, *Nano Energy*, 2017, **34**, 408–420.
15 C. Lu, X. Jiang, W. Sun, Z. Wang, K. Sun, D. W. Rooney and J. Wang, *J. Mater. Chem. A*, 2017, **5**, 24636–24644.
16 Y. Duan, B. Zhang, J. Zheng, J. Hu, J. Wen, D. J. Miller, P. Yan, T. Liu, H. Guo, W. Li, X. Song, Z. Zhuo, C. Liu, H. Tang, R. Tan, Z. Chen, Y. Ren, Y. Lin, W. Yang, C. M. Wang, L. W. Wang, J. Lu, K. Amine and F. Pan, *Nano Lett.*, 2017, **17**, 6018–6026.
17 H. Wang, N. Zhao, C. Shi, L. Ma, F. He, C. He, J. Li and E. Liu, *Electrochim. Acta*, 2017, **247**, 1030–1037.
18 Y. Duan, L. Yang, M. J. Zhang, Z. Chen, J. Bai, K. Amine, F. Pan and F. Wang, *J. Mater. Chem. A*, 2019, **7**, 513–519.
19 M.-J. Zhang, X. Hu, M. Li, Y. Duan, L. Yang, C. Yin, M. Ge, X. Xiao, W.-K. Lee, J. Y. P. Ko, K. Amine, Z. Chen, Y. Zhu, E. Dooryhee, J. Bai, F. Pan and F. Wang, *Adv. Energy Mater.*, 2019, 1901915.
20 Z. Wu, S. Ji, J. Zheng, Z. Hu, S. Xiao, Y. Wei, Z. Zhuo, Y. Lin, W. Yang, K. Xu, K. Amine and F. Pan, *Nano Lett.*, 2015, **15**, 5590–5596.
21 Y. Li, H. Chen, K. Lim, H. D. Deng, J. Lim, D. Fraggedakis, P. M. Attia, S. C. Lee, N. Jin, J. Moškon, Z. Guan, W. E. Gent, J. Hong, Y. S. Yu, M. Gaberšček, M. S. Islam, M. Z. Bazant and W. C. Chueh, *Nat. Mater.*, 2018, **17**, 915–922.
22 J. Zheng, Y. Hou, Y. Duan, X. Song, Y. Wei, T. Liu, J. Hu, H. Guo, Z. Zhuo, L. Liu, Z. Chang, X. Wang, D. Zherebetskyy, Y. Fang, Y. Lin, K. Xu, L. W. Wang, Y. Wu and F. Pan, *Nano Lett.*, 2015, **15**, 6102–6109.
23 X. Song, T. Liu, J. Amine, Y. Duan, J. Zheng, Y. Lin and F. Pan, *Nano Energy*, 2017, **37**, 90–97.
24 W. Tang, X. Song, Y. Du, C. Peng, M. Lin, S. Xi, B. Tian, J. Zheng, Y. Wu, F. Pan and K. P. Loh, *J. Mater. Chem. A*, 2016, **4**, 4882–4892.
25 J. Hu, W. Li, Y. Duan, S. Cui, X. Song, Y. Liu, J. Zheng, Y. Lin and F. Pan, *Adv. Energy Mater.*, 2017, **7**, 1601894.
26 J. Hu, W. Ren, X. Chen, Y. Li, W. Huang, K. Yang, L. Yang, Y. Lin, J. Zheng and F. Pan, *Nano Energy*, 2020, **74**, 104864.
27 W. Zhang, X. Sun, Y. Tang, H. Xia, Y. Zeng, L. Qiao, Z. Zhu, Z. Lv, Y. Zhang, X. Ge, S. Xi, Z. Wang, Y. Du and X. Chen, *J. Am. Chem. Soc.*, 2019, **141**, 14038–14042.
28 P. Bai and M. Z. Bazant, *Nat. Commun.*, 2014, **5**, 3585.
29 H. Wang, R. Wang, L. Liu, S. Jiang, L. Ni, X. Bie, X. Yang, J. Hu, Z. Wang, H. Chen, L. Zhu, D. Zhang, Y. Wei, Z. Zhang, S. Qiu and F. Pan, *Nano Energy*, 2017, **39**, 346–354.
30 W. Ren, K. Wang, J. Yang, R. Tan, J. Hu, H. Guo, Y. Duan, J. Zheng, Y. Lin and F. Pan, *J. Power Sources*, 2016, **331**, 232–239.
31 Y. Liu, J. Liu, J. Wang, M. N. Banis, B. Xiao, A. Lushington, W. Xiao, R. Li, T. K. Sham, G. Liang and X. Sun, *Nat. Commun.*, 2018, **9**, 929.
32 D. Lepage, C. Michot, G. Liang, M. Gauthier and S. B. Schougaard, *Angew. Chemie - Int. Ed.*, 2011, **50**, 6884–6887.
33 L. Guo, Y. Zhang, J. Wang, L. Ma, S. Ma, Y. Zhang, E. Wang, Y. Bi, D. Wang, W. C. McKee, Y. Xu, J. Chen, Q. Zhang, C. Nan, L. Gu, P. G. Bruce and Z. Peng, *Nat. Commun.*, 2015, **6**, 7898.
34 K. S. Park, P. Xiao, S. Y. Kim, A. Dylla, Y. M. Choi, G. Henkelman, K. J. Stevenson and J. B. Goodenough, *Chem. Mater.*, 2012, **24**, 3212–3218.
35 Y. Li, Y. Zhang, J. Ma, L. Yang, X. Li, E. Zhao, S. Fan, G. Xu, S. Yang and C. Yang, *J. Electrochem. Soc.*, 2019, **166**, A410–A415.
36 Z. Wu, X. Han, J. Zheng, Y. Wei, R. Qiao, F. Shen, J. Dai, L. Hu, K. Xu, Y. Lin, W. Yang and F. Pan, *Nano Lett.*, 2014, **14**, 4700–4706.
37 D. Aurbach, B. Markovsky, G. Salitra, E. Markevich, Y. Talyossef, M. Koltypin, L. Nazar, B. Ellis and D. Kovacheva, *J. Power Sources*, 2007, **165**, 491–499.
38 J. Wang, Y. Tang, J. Yang, R. Li, G. Liang and X. Sun, *J. Power Sources*, 2013, **238**, 454–463.
39 W. Huang, J. Hu, L. Yang, W. Zhao, Z. Wang, H. Wang, Z. Guo, Y. Li, J. Liu, K. Yang and F. Pan, *ACS Appl. Mater. Interfaces*, 2019, **11**, 957–962.
40 T. Liu, A. Dai, J. Lu, Y. Yuan, Y. Xiao, L. Yu, M. Li, J. Gim, L. Ma, J. Liu, C. Zhan, L. Li, J. Zheng, Y. Ren, T. Wu, R. Shahbazian-Yassar, J. Wen, F. Pan and K. Amine, *Nat. Commun.*, 2019, **10**, 1–11.
41 Y. Wu, L. Ben, H. Yu, W. Qi, Y. Zhan, W. Zhao and X. Huang, *ACS Appl. Mater. Interfaces*, 2019, **11**, 6937–6947.
42 P. Yan, J. Zheng, J. Liu, B. Wang, X. Cheng, Y. Zhang, X. Sun, C. Wang and J. G. Zhang, *Nat. Energy*, 2018, **3**, 600–605.
43 G. L. Xu, Q. Liu, K. K. S. Lau, Y. Liu, X. Liu, H. Gao, X. Zhou, M. Zhuang, Y. Ren, J. Li, M. Shao, M. Ouyang, F. Pan, Z. Chen, K. Amine and G. Chen, *Nat. Energy*, 2019, **4**, 484–494.
44 L. Yang, Y. Xia, L. Qin, G. Yuan, B. Qiu, J. Shi and Z. Liu, *J. Power Sources*, 2016, **304**, 293–300.
45 Y. K. Sun, Z. Chen, H. J. Noh, D. J. Lee, H. G. Jung, Y. Ren, S. Wang, C. S. Yoon, S. T. Myung and K. Amine, *Nat. Mater.*, 2012, **11**, 942–947.
46 D. Kong, J. Hu, Z. Chen, K. Song, C. Li, M. Weng, M. Li, R. Wang, T. Liu, J. Liu, M.-J. Zhang, Y. Xiao and F. Pan, *Adv. Energy Mater.*, 2019, 1901756.
47 Q. Wei, X. Wang, X. Yang, B. Ju, B. Hu, H. Shu, W. Wen, M. Zhou, Y. Song, H. Wu and H. Hu, *J. Mater. Chem. A*, 2013, **1**, 4010–4016.
48 S. M. Oh, S. T. Myung, J. B. Park, B. Scrosati, K. Amine and Y. K. Sun, *Angew. Chemie - Int. Ed.*, 2012, **51**, 1853–1856.
49 K. J. Kreder and A. Manthiram, *ACS Energy Lett.*, 2017, **2**, 64–69.
50 Z. Wu, S. Ji, T. Liu, Y. Duan, S. Xiao, Y. Lin, K. Xu and F. Pan, *Nano Lett.*, 2016, **16**, 6357–6363.

This journal is © The Royal Society of Chemistry 20xx

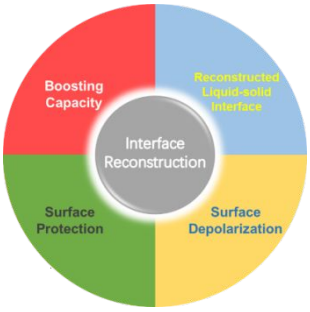

The impact of surface structure and interface reconstruction of lithium-ion battery cathode materials on their electrochemical performances is summarized.